ICNMM2009-82194

LIQUID FILM THICKNESS IN MICRO TUBE UNDER FLOW BOILING CONDITION

Youngbae Han and Naoki Shikazono
Department of Mechanical Engineering,
The University of Tokyo,
Hongo 7-3-1, Bunkyo-ku, Tokyo, Japan

ABSTRACT

Slug flow is one of the representative flow regimes of flow boiling in micro tubes. It is well known that the thin liquid film formed between the tube wall and the vapor bubble plays an important role in micro scale heat transfer. In the previous study [1], liquid film thickness under adiabatic condition was investigated and an empirical correlation for the initial liquid film thickness based on capillary number, Reynolds number and Weber number was proposed. In the present study, the effects of wall superheat and bubble acceleration on the liquid film thickness are investigated. Under flow boiling condition, bubble velocity is not constant but accelerated, and it is necessary to consider this acceleration effect on the liquid film thickness, since it may affect the viscous, surface tension and inertia forces in the momentum equation. In addition, viscous boundary layer develops, and it may also affect the liquid film thickness. Besides, viscosity and surface tension coefficient are sensitive to temperature change. If wall superheat is high, it is crucial to consider the property change according to the temperature variation. In order to investigate these effects, laser focus displacement meter is used to measure the liquid film thickness. Ethanol, water and FC-40 are used as working fluids. Circular tubes with three different diameters, D = 0.5, 0.7 and 1.0 mm, are used. It is observed that when the wall superheat is larger than 5°C, liquid film thickness becomes thinner than the adiabatic case due to the decrease of viscosity near the wall. The increase of liquid film thickness with capillary number is restricted by bubble acceleration. Finally, an empirical correlation is proposed for accelerated flows in terms of capillary number and Bond number based on bubble acceleration.

NOMENCLATURE

Symbol	Description	Unit
Bo	Bond number	-
Ca	capillary number	-
D	tube diameter	m
G	mass flow rate	kg/m^{2}s
h	convection heat transfer coefficient	W/m^{2}K
I	current	A
k	thermal conductivity	W/mK
l	heating length	m
L	distance from the measuring point	m
n	refractive index	-
q''	heat flux	W/m^2
R	tube radius	m
Re	Reynolds number	-
T	temperature	°C
U	bubble velocity	m/s
V	voltage	V
We	Weber number	-

Greek Symbols

δ	liquid film thickness	m
δ^*	viscous boundary layer thickness	m
λ	transition region length	
μ	viscosity	Pa·s
ν	kinematic viscosity	m^2/s
ρ	density	kg/m^3
σ	surface tension coefficient	N/m

Subscripts

0	initial
air	air
in	inner
inlet	inlet of test tube
loss	loss
out	outer
outlet	outlet of test tube
sat	saturated
super	superheat
wall	tube wall

1. INTRODUCTION

Micro scale heat transfer attracts large attention due to its many advantages, e.g., high efficiency, miniaturization, etc. However, the characteristics of two-phase flow in micro tubes are quite different from those in conventional tubes and they

are not fully understood. Flow regimes are also different in micro tubes due to surface tension, and slug flow becomes one of the dominant flow patterns. It is well known that the thin liquid film formed between the tube wall and the vapor bubble plays an important role in micro tube heat transfer. It is reported that the thickness of the liquid film is one of the important parameters for the prediction of flow boiling heat transfer in micro tubes [2,3].

Many researches have been conducted both experimentally and theoretically to investigate the liquid film thickness in slug flow. Taylor [4] experimentally obtained the mean liquid film thickness remaining on the wall by measuring the difference of the bubble velocity and the mean velocity. Highly viscous fluids, i.e., glycerin, syrup-water mixture and lubricating oil, were used so that wide capillary number range could be covered. It is reported that the liquid film thickness increases with capillary number and reaches a certain fraction of the tube diameter. Bretherton [5] analytically investigated the liquid film thickness and axial pressure drop across the bubble with the lubrication equations. Assuming small capillary number, it is shown that the dimensionless liquid film thickness can be scaled with $Ca^{2/3}$.

Moriyama et al. [6] obtained the liquid film thickness formed by a vapor bubble expansion in a narrow gap by measuring the temperature change of the channel wall which was initially superheated. In their experiment, it was assumed that the whole liquid film on the wall evaporates and the heat is consumed by the evaporation of the liquid film. It is reported that when the acceleration becomes large, liquid film thickness is determined by the viscous boundary layer thickness. Their experimental data was correlated in terms of capillary number and Bond number based on the interface acceleration. Heil [7] numerically investigated the effect of inertia force on the liquid film thickness. It is shown that the liquid film thickness and the pressure gradient depend on Reynolds number. Aussillous and Quere [8] measured the liquid film thickness using fluids with relatively low surface tension. It was found that the liquid film thickness deviates from the Taylor's data at relatively high capillary numbers. Visco-inertia regime where the effect of inertia force on the liquid film thickness becomes significant was demonstrated. It was also observed that the liquid film thickness is determined by the viscous boundary layer when viscous boundary layer thickness is thin. Kreutzer et al. [9] investigated the liquid film thickness and the pressure drop in a micro tube both numerically and experimentally. Predicted liquid film thickness showed almost the same trend with that reported by Heil [7].

Utaka et al. [10] measured the liquid film thickness formed by a vapor bubble in a narrow gap mini-channel with laser extinction method. It was concluded that the boiling phenomena were determined by two characteristic periods, i.e., the micro-layer dominant and the liquid saturated periods. Han and Shikazono [1] measured the liquid film thickness in micro tube locally and instantaneously under adiabatic condition with laser focus displacement meter. The effect of inertia force on the liquid film thickness was investigated using micro tubes with different diameters and several working fluids. An empirical correlation based on capillary number, Reynolds number and Weber number was proposed.

Although many experiments have been carried out to measure the liquid film thickness in micro tubes, most of the experiments were conducted under adiabatic condition. However, under flow boiling condition, the bubble velocity is not constant but accelerated, and it is necessary to consider this acceleration effect on the liquid film thickness, since it may affect the viscous, surface tension and inertia forces in the momentum equation. In addition, viscous boundary layer develops, and it may also affect the liquid film thickness. Besides, viscosity and surface tension are sensitive to temperature change. If the wall superheat is high, it is crucial to consider the property change according to the temperature variation. In the present study, the effects of bubble acceleration and the wall superheat on the liquid film thickness are investigated experimentally.

2. EXPERIMENTAL SETUP AND PROCEDURES

2.1 The wall superheat and the bubble acceleration

Liquid film thickness under adiabatic condition is determined by the force balance among viscous, surface tension and inertia forces. However, under flow boiling condition, the effects of wall superheat and bubble acceleration must be considered. In order to investigate each of these effects independently, two experimental setups were used in the present study.

Circular tubes made of Pyrex glass with inner diameters of 0.5, 0.7 and 1.0 mm were used as test tubes. Tube diameter was measured with a microscope and the averaged value of the inlet and outlet inner diameters was used for the analysis. Figure 1 and Table 1 show the photograph of the 0.487 mm inner diameter tube and the dimensions of the micro tubes. The differences of inlet and outlet inner diameters are less than 1% for all tubes. Ethanol, water and FC-40 were used as the working fluids. For the wall superheat experiment, only the micro tube of inner diameter 0.5 mm and ethanol were used.
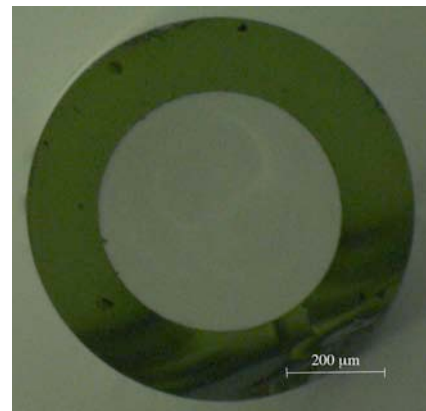

Fig. 1 Cross section of the 0.487 mm inner diameter tube.

Table 1 Dimensions of the micro tubes.

Circular tube		
I.D. (mm)	O.D. (mm)	Length (mm)
0.995	1.6	250
0.715	1.0	250
0.487	0.8	250

2.2 Experimental setup for the wall superheat

Figure 2 shows the schematic diagram of the wall superheat experimental setup. In Fig. 2, working fluid is degassed by a degasser and pumped at a uniform flow rate with a plunge pump. In the preheater, ethanol is heated up to the saturated temperature and small vapor bubble is generated periodically. Generated vapor bubble in the preheater flows into the test tube which is superheated initially and expands due to the evaporation. Test tube is coated by ITO, which is a transparent conductive film for Joule heating. ITO film is connected to the DC power supply. Heat flux to the working fluid is obtained as follows:

$$q''(x) = \frac{VI}{l \cdot \pi D_{in}} - q''_{loss}(x), \qquad (1)$$

$$q''_{loss}(x) = h(x) \cdot \left(T_{wall\_out} - T_{air}\right), \qquad (2)$$

where $q''(x)$ is local heat flux, V is voltage, I is current, l is heating length, D_{in} is inner diameter and $q''_{loss}(x)$ is local heat loss. Local natural convection heat transfer coefficient $h(x)$ is obtained from the heat loss experiment and its range is from 30 to 50 W/m²K in the present experiment. T_{wall_out} and T_{air} are temperatures of outer wall and air, respectively. Outer wall temperatures are measured by K-type thermocouples calibrated within ±0.1°C error, and inner wall temperatures are calculated from the 1D heat conduction equation as follows:

$$T_{wall\_in} = T_{wall\_out} - \frac{q''(x)}{k} \frac{D_{in}}{2} \cdot \ln\left(\frac{D_{out}}{D_{in}}\right), \qquad (3)$$

where k is thermal conductivity of Pyrex glass. Figure 3 shows the heating length and measuring points in the test section.

The velocity of the vapor bubble is measured from the images captured by the high-speed camera (Phantom 7.1). The images are taken at several frame rates according to the bubble velocity. For the maximum bubble velocity, frame rate is 10000 frames per second with a shutter time of 10 µs. Laser focus displacement meter (hereafter LFDM; LT9010M, Keyence) is used to measure the liquid film thickness. LFDM has been used by several researchers for liquid film thickness measurements [11, 12]. It is reported that LFDM can measure the liquid film thickness very accurately within 1% error [11]. Figure 4 shows the principle of the LFDM. The position of the target surface can be determined by the displacement of objective lens moved by the tuning fork. The intensity of the reflected light becomes highest in the light-receiving element when the focus is obtained on the target surface. Objective lens is vibrated continually in the range of ±0.3 mm. For transparent materials, relative distances between interfaces can be detected during one cycle of the objective lens vibration. The resolution of the present laser focus displacement meter is 0.01 µm, the laser spot diameter is 2 µm and the response time is 640 µs. Thus, it is possible to measure the liquid film thickness instantaneously and locally. Measured liquid film thickness is transformed to DC voltage signal in the range of ±10V. Output signal was sent to PC through GPIB interface and recorded with LabVIEW.
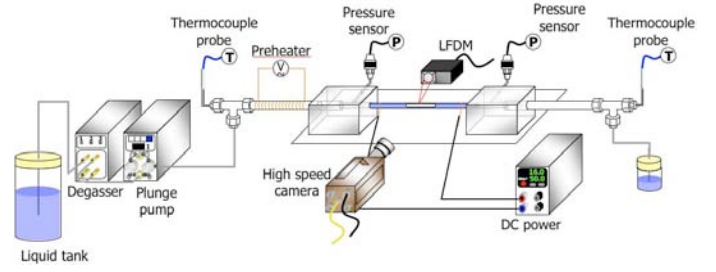

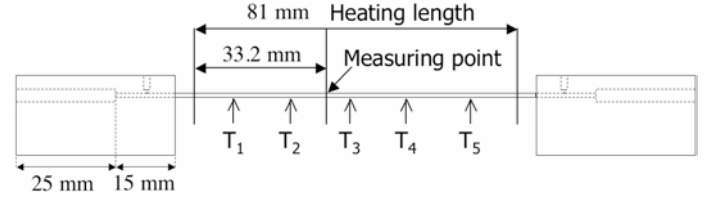**Fig. 2** Schematic diagram of the experimental setup for the wall superheat.

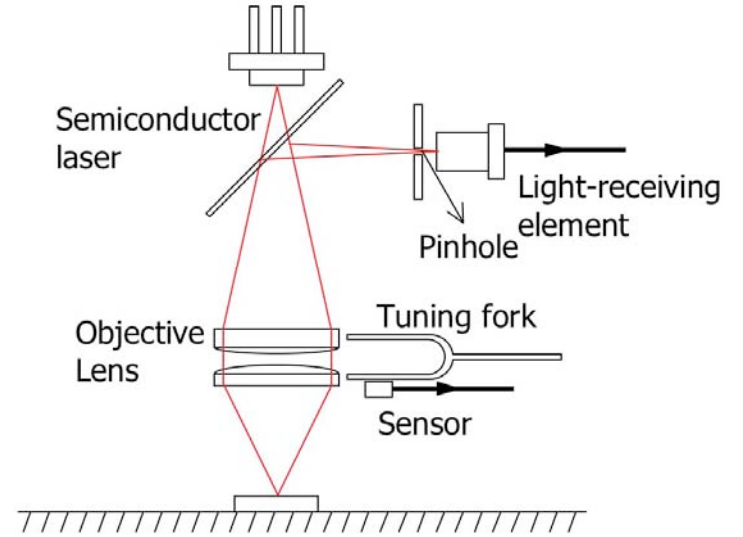**Fig. 3** Measuring points and heating length in the test section.

Fig. 4 Principle of laser focus displacement meter.

2.3 Experimental setup for the adiabatic bubble acceleration

In order to investigate the effect of bubble acceleration on the liquid film thickness without the effect of temperature gradient, adiabatic bubble acceleration experiment is conducted. Figure 5 shows the schematic diagram of the bubble acceleration experimental setup. One side of Pyrex glass tube is connected to the syringe. Actuator motor (EZHC6A-101, Oriental motor) is used to pull the liquid in the micro tube. The velocity range of the actuator motor is from 0 to 0.2 m/s. Syringes with several cross sectional areas are used to control the liquid velocity in the test section. Thus, the range of bubble velocity in the present experiment is varied from 0 to 7 m/s. High-speed camera is used to measure the bubble velocity and acceleration. LFDM is used to measure the liquid film thickness.
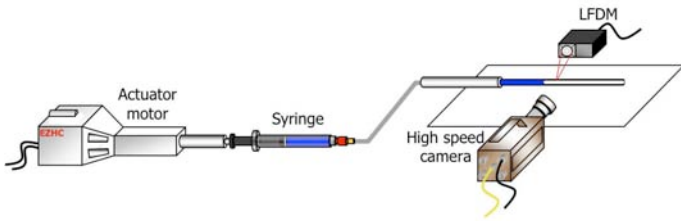
Fig. 5 Schematic diagram of the experimental setup for the adiabatic bubble acceleration.
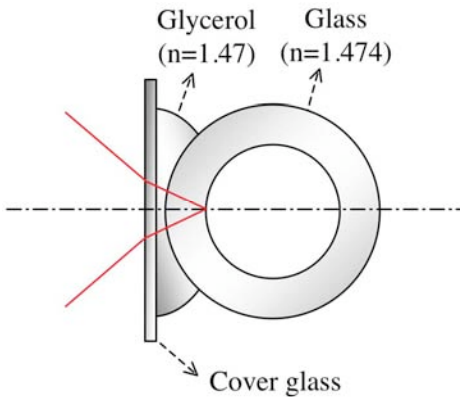

Fig. 6 Correction for the outer wall curvature.

2.4 Correction for the tube wall curvature

As the laser beam passes through the tube wall, focus is scattered within a certain range due to the difference of curvatures between axial and azimuthal directions. Cover glass and glycerol were used to remove the curvature effect caused by the outer wall as shown in Fig. 6. Refractive index of glycerol ($n = 1.47$) is almost the same with that of the Pyrex glass ($n = 1.474$), so the refraction of laser between glycerol and Pyrex glass can be neglected. Refractive indices of ethanol, water and FC-40 are 1.36, 1.33 and 1.29 under the condition of 1 atm and 25°C. It is difficult to detect the interface between inner wall and liquid, because the difference of the refractive indices of the wall and the liquid is small. Therefore, the distance from the cover glass to the dry inner wall is initially measured without flowing the liquid. Then, the thickness with liquid film is measured. The liquid film thickness is calculated from the difference of these two values.

The effect of the inner wall curvature is corrected by the equation suggested by Takamasa and Kobayashi [12]. The curvature effect caused by inner wall is not so severe when the liquid film is thin. The scattering length is less than 2% of the liquid film thickness in the present study.

2.5 Experimental procedure for the wall superheat

Figures 7 and 8 shows a typical measurement example. Figure 7 shows the variation of temperature at each measuring point. Vapor bubble generated in preheater flows into test tube periodically and boiling takes place in the test section. It is reported that vapor bubble is not generated in a micro tube until the wall superheat becomes quite high. In the present experiments, vapor bubbles are not generated in micro tube until the wall superheat becomes more than 35°C. Therefore, flow in micro tube becomes a superheated liquid flow. Figure 8

shows the variation of liquid film thickness with time when the vapor bubble expands. If the micro tube is filled with liquid at the measuring point, there is no signal for the liquid film thickness from LFDM. After bubble nose passes by the measuring point, liquid film is formed on the tube wall and the signal for the liquid film thickness can be obtained. Bubble velocity and acceleration are calculated from the images captured by high-speed camera. In order to exclude the effect of acceleration on the liquid film thickness, experimental data with small acceleration values are adopted for the wall superheat experiment. In Fig. 8, unlike the adiabatic condition, liquid film thickness does not become constant but decreases due to the evaporation and shows slight scattering.
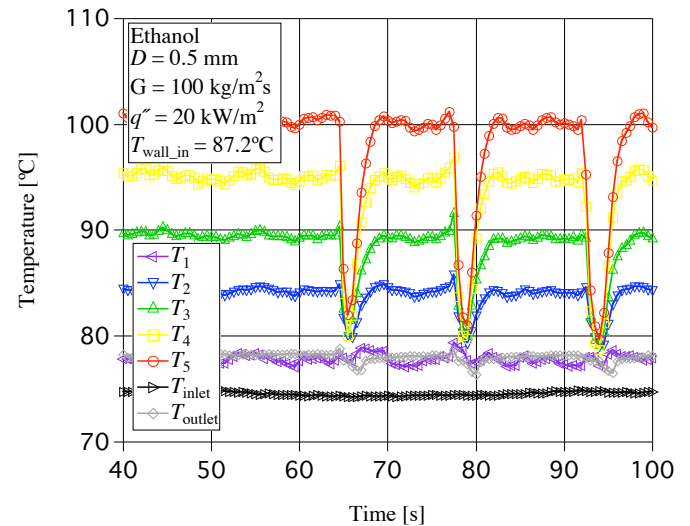

Fig. 7 Inner wall temperature against time, ethanol, $D = 0.5$ mm, $G = 100$ kg/m^{2}s, $q'' = 20$ kW/m^2, T_{wall_in} at the measuring point = 87.2°C
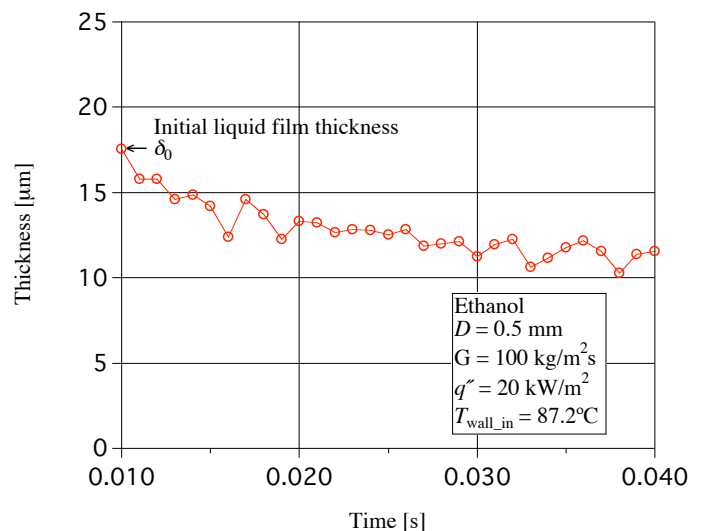

Fig. 8 Liquid film thickness against time, ethanol, $D = 0.5$ mm, $G = 100$ kg/m^{2}s, $q'' = 20$ kW/m^2, T_{wall_in} at the measuring point = 87.2°C

2.6 Experimental procedure for the adiabatic bubble acceleration

In order to investigate the effect of bubble acceleration on the liquid film thickness, measuring points are positioned at $L = 5, 10$ and 20 mm away from the air-liquid as shown in Fig. 9. For each location, liquid is accelerated to a certain velocity with the actuator motor. Figures 10 and 11 show a typical measurement example in the adiabatic bubble acceleration experiment. Figure 10 shows bubble velocity against time at $L = 20$ mm. Bubble velocity at $L = 20$ mm is obtained from the velocity fitting curve. Figure 11 shows the time variation of liquid film thickness for the case of Fig. 10. After the initial quick decrease, liquid film thickness decreases gradually with time. After the liquid film is formed, liquid film is driven by the shear force of gas flow. For a constant bubble velocity, initial liquid film thickness doesn't depend on measuring location. However, when the flow is accelerated, liquid film thickness increases with the distance from the initial bubble location.

3. RESULTS AND DISCUSSION

3.1 The effect of the wall superheat

Figure 12 shows the dimensionless liquid film thickness against capillary number in the wall superheat experiments. Solid line in Fig. 12 is an empirical correlation [1] for the initial liquid film thickness under adiabatic condition, which is written as follows:

$$\frac{\delta_0}{D} = \begin{cases} \dfrac{0.670 Ca^{\frac{2}{3}}}{1+3.13 Ca^{\frac{2}{3}}+0.504 Ca^{0.672} Re^{0.589}-0.352 We^{0.629}} & (Re < 2000) \\[4mm] \dfrac{106.0\left(\frac{\mu^2}{\rho\sigma}\cdot\frac{1}{D}\right)^{\frac{2}{3}}}{1+497.0\left(\frac{\mu^2}{\rho\sigma}\cdot\frac{1}{D}\right)^{\frac{2}{3}}+7330\left(\frac{\mu^2}{\rho\sigma}\cdot\frac{1}{D}\right)^{0.672}-5000\left(\frac{\mu^2}{\rho\sigma}\cdot\frac{1}{D}\right)^{0.629}} & (Re > 2000). \end{cases} \quad (4)$$

Under adiabatic condition, liquid film thickness is determined by capillary, Reynolds and Weber numbers for $Re < 2000$. Liquid film thickness becomes constant for $Re > 2000$. Detailed explanation for Equation (4) can be found in [1].

Properties at saturated temperature are used for the prediction in Fig. 12. Square open marks represent the data of the wall superheat less than 5°C, and they follow the adiabatic prediction very well. However, as the wall superheat increases, liquid film thickness becomes thinner than the adiabatic prediction. It is considered that the liquid viscosity near the wall decreases due to the increase of wall temperature. It is known that the liquid film thickness is determined by force balance among viscous, surface tension and inertia forces. Density, surface tension coefficient and viscosity are main properties. Density is not so sensitive to temperature, and thus the change of inertia force is not so large. Surface tension force works on the liquid-vapor interface and the interface temperature is considered to be the saturated temperature. Therefore, Surface tension force is not affected so largely by the wall superheat. On the other hand, viscous force becomes important near the wall. Viscosity is sensitive to temperature change and decreases with the wall superheat. As viscosity decreases, viscous force becomes weak and liquid film thickness also decreases.
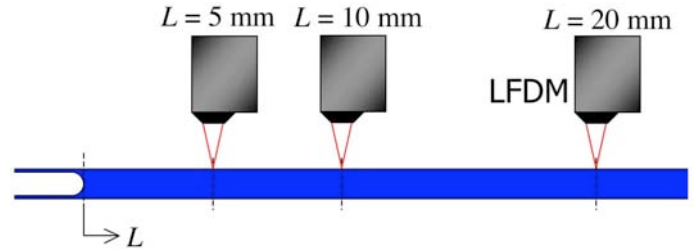

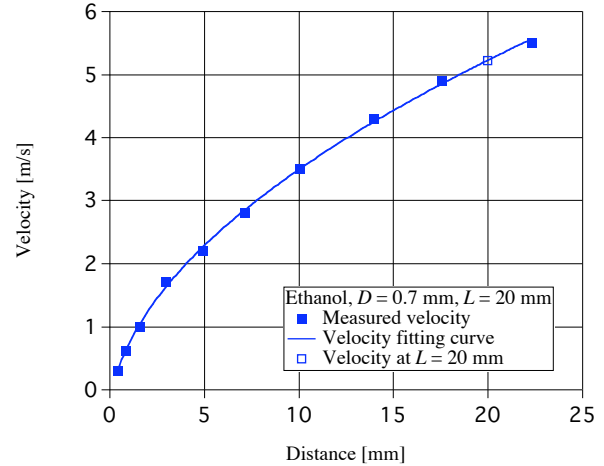**Fig. 9** Initial bubble location $L = 0$ and the measuring points, $L = 5, 10$ and 20 mm.

Fig. 10 Measured bubble velocity against distance from the initial bubble location, $U = 5.22$ m/s.
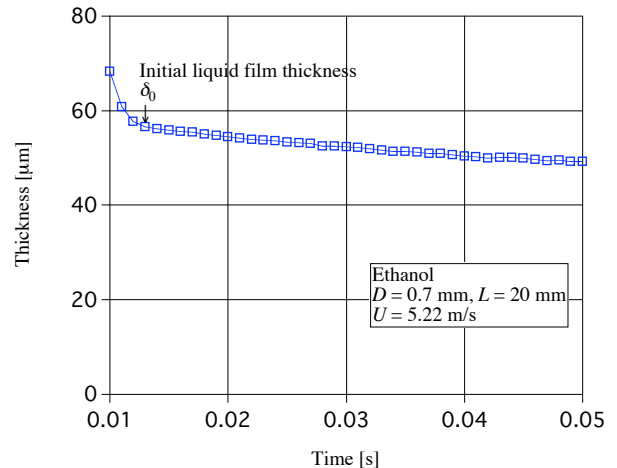

Fig. 11 Liquid film thickness against time, ethanol, $D = 0.7$ mm, $L = 20$ mm, $U = 5.22$ m/s.

Figure 13 shows the comparison between predicted liquid film thicknesses using Eq. (4) and the experimental data. Liquid properties of saturated temperature are used for the open square symbols and it is shown that the prediction overestimates the experimental data. If the wall temperature is used for the viscosity, agreement between prediction and experiment becomes better as shown by the open circular marks. Therefore, if the wall superheat is high, it is recommended to use viscosity defined at wall temperature for the prediction.
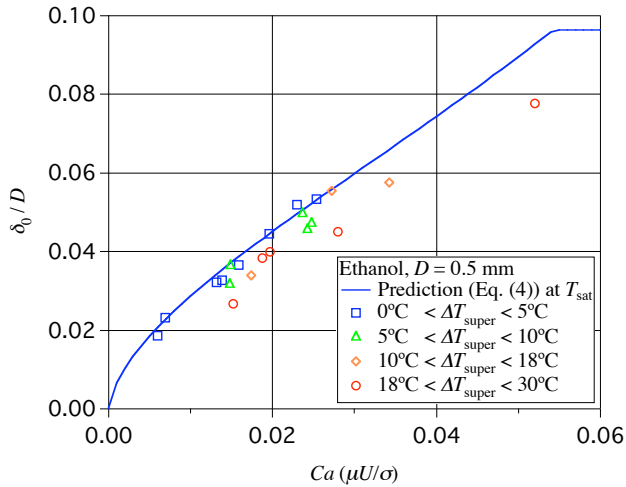
5

Fig. 12 Deviation from prediction value according to the wall superheat, ethanol, $D = 0.5$ mm.
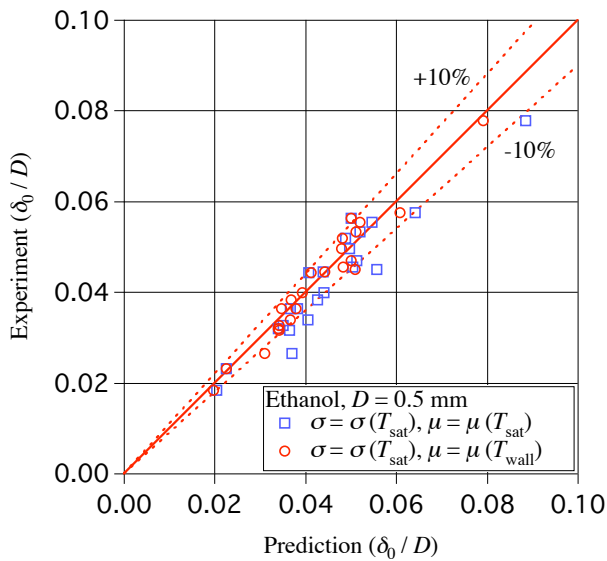

Fig. 13 Comparison of prediction and experimental results.

3.2 The effect of the bubble acceleration

Figure 14 shows the dimensionless liquid film thickness against capillary number using ethanol. Distance from the initial bubble location is fixed, and thus acceleration is larger for larger capillary numbers. Liquid film thickness is identical with the zero acceleration curve at small capillary number. However, as capillary number increases, liquid film thickness becomes constant and is much smaller than the zero acceleration data. For $D = 0.7$ and 1.0 mm tubes, liquid film thickness shows slight decrease with capillary number. It is considered that viscous boundary layer developed by bubble acceleration affects the liquid film thickness. It is reported in previous researches [6,8] that the liquid film thickness is restricted by the viscous boundary layer when viscous boundary layer thickness is very thin. Even though viscous boundary layer thickness has no relation to tube diameter, absolute liquid film thickness increases as tube diameter increases at the same velocity and distance in the present

experiments. It is considered that liquid film thickness is not only affected by the viscous boundary layer but also by surface tension force If the viscous boundary layer is thick, liquid film thickness is identical with the zero acceleration case.
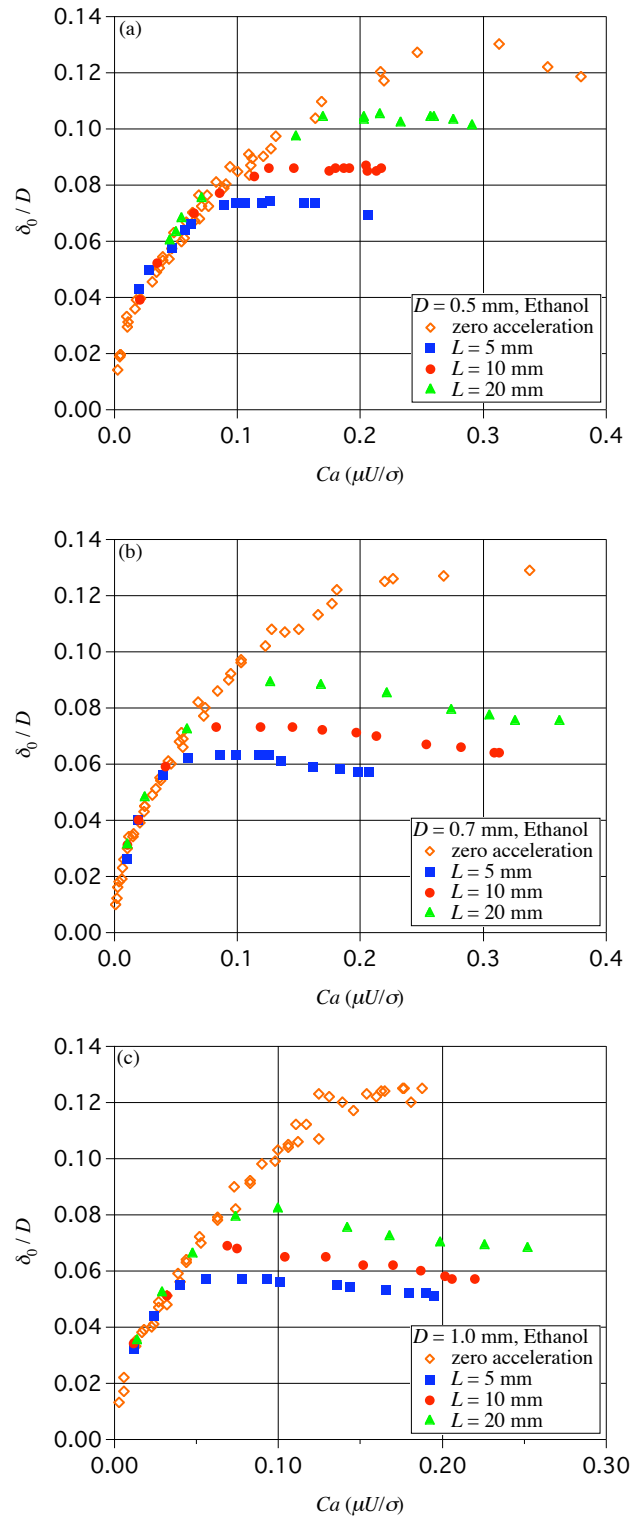

Fig. 14 Dimensionless liquid film thickness (δ_0/D) against capillary number ($Ca = \mu U/\sigma$) at different measuring points using ethanol, $L = 5$, 10 and 20 mm, (a) $D = 0.5$ mm, (b) $D = 0.7$ mm, (c) $D = 1.0$ mm.

If the viscous boundary layer is thin, force balance is affected by the viscous boundary layer and liquid film thickness should deviate from the zero acceleration case. The force balance altered by viscous boundary layer determines liquid film thickness.

Figure 15 shows the dimensionless liquid film thickness against capillary number using water. As the case of ethanol, liquid film thickness can be divided into two regions. Liquid film thickness becomes identical with the zero acceleration data at small capillary number.
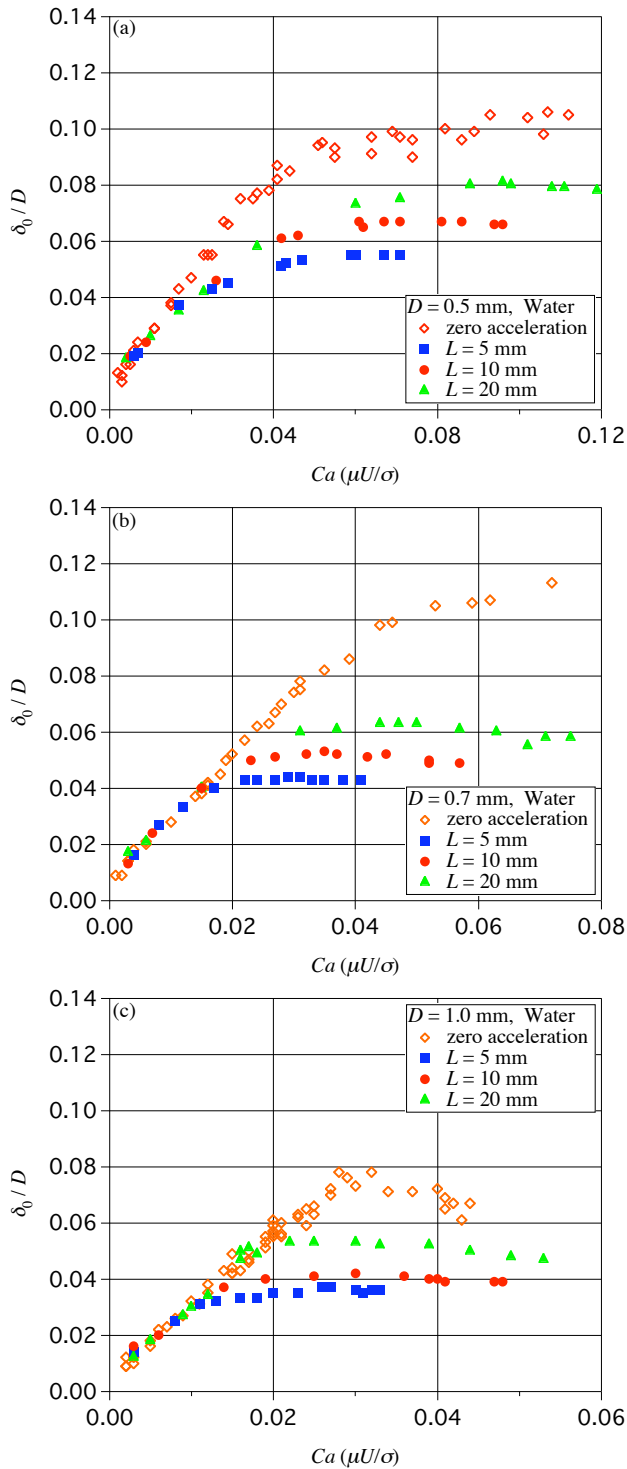

Fig. 15 Dimensionless liquid film thickness (δ_0/D) against capillary number ($Ca = \mu U/\sigma$) at different measuring points using water, L = 5, 10 and 20 mm, (a) D = 0.5 mm, (b) D = 0.7 mm, (c) D = 1.0 mm.
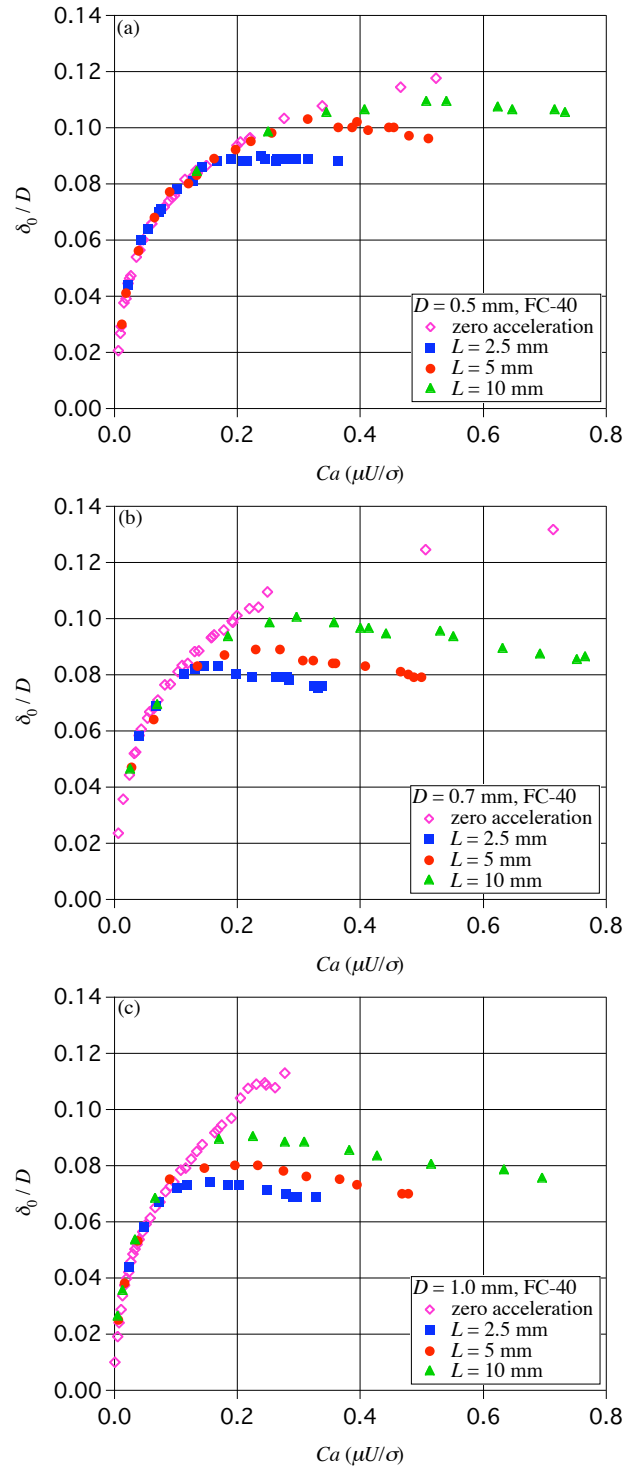
Fig. 16 Dimensionless liquid film thickness (δ_0/D) against capillary number ($Ca = \mu U/\sigma$) at different measuring points using FC-40, L = 2.5, 5 and 10 mm, (a) D = 0.5 mm, (b) D = 0.7 mm, (c) D = 1.0 mm.

As capillary number increases, liquid film thickness deviates from the zero acceleration case. For ethanol, liquid film thickness shows slight decrease with capillary number. On the contrary, in case of water, liquid film thickness increases continually after it deviates from the zero acceleration case. This different trend is apparent especially in $D = 0.5$ mm case. Surface tension force works most strongly in the case of water and tube diameter $D = 0.5$ mm. Therefore, this different trend has a relation to surface tension.

Figure 16 shows the dimensionless liquid film thickness against capillary number using FC-40. Viscous boundary layer grows quickly in FC-40 due to its large viscosity. In order to obtain thinner viscous boundary layer, measuring point is changed as $L = 2.5$, 5, 10 mm. Liquid film thickness is also divided into two regions. Due to small surface tension of FC-40, liquid film thickness decreases with capillary number after deviation from the zero acceleration data.

Viscous boundary layer thickness can be scaled as follows:

$$\delta^* \sim \left(\frac{\nu L}{U}\right)^{1/2}, \tag{5}$$

where δ^* is viscous boundary layer thickness, ν is kinematic viscosity, L is the distance from the starting point and U is velocity. Figure 17 shows dimensionless liquid film thickness against dimensionless viscous boundary layer thickness.
In Fig. 17, it is shown that experimental values approach asymptotic lines when the viscous boundary layer thickness is thin. These lines correspond to the restriction on the liquid film thickness caused by the viscous boundary layer. These restriction lines are different between different working fluids. At the same viscous boundary layer thickness, dimensionless liquid film thickness becomes thinner for water.

3.3 Scaling analysis for the bubble acceleration

Aussillous and Quere [8] made a scaling analysis on the liquid film thickness based on Bretherton's theoretical analysis [5]. The momentum balance and the curvature matching between the bubble nose and the transition region are expressed as follows:

$$\frac{\mu U}{\delta_0^2} \sim \frac{1}{\lambda}\left\{\frac{\sigma}{R - \delta_0}\right\}, \tag{6}$$

$$\frac{\delta_0}{\lambda^2} \sim \frac{1}{R - \delta_0}, \tag{7}$$

where λ is transition region length and R is tube radius. The relation δ_0/D is deduced as follows:

$$\frac{\delta_0}{D} \sim \frac{Ca^{2/3}}{1 + Ca^{2/3}}. \tag{8}$$

Based on Eq. (8), Taylor's experimental data was fitted as follows [8]:

$$\frac{\delta_0}{D} = \frac{0.67 Ca^{2/3}}{1 + 3.35 Ca^{2/3}}. \tag{9}$$

Equation (9) is called the Taylor's law.

Figure 18 shows the schematic diagram of velocity profiles under steady and acceleration conditions. Under bubble acceleration condition, bubble nose curvature is affected by the thin viscous boundary layer. This is considered to be the reason for the decrease of the liquid film thickness under bubble acceleration condition. Under acceleration, the bubble nose curvature is modified as:

$$\kappa \sim \left(\frac{1}{R - \delta_0}\right) \cdot f. \tag{10}$$

If the bubble nose curvature is replaced with Eq. (10), Eq. (8) is changed as follows:

$$\frac{\delta_0}{D} \sim \frac{Ca^{2/3} \cdot f^{-1}}{1 + Ca^{2/3} \cdot f^{-1}}. \tag{11}$$

Eq. (11) can be rewritten as:

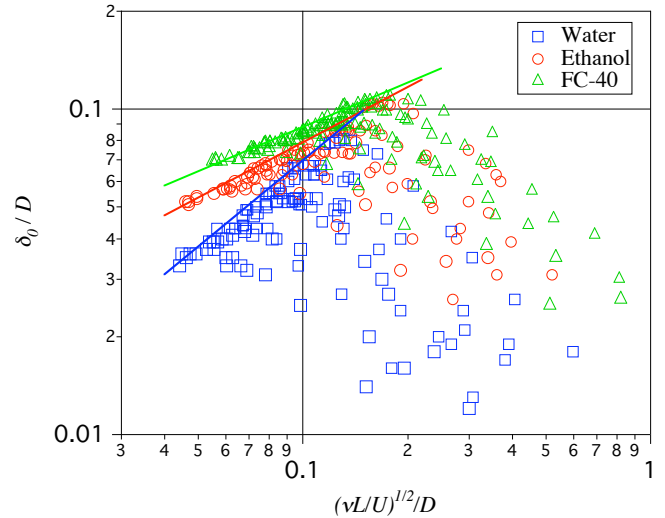$$f \sim \frac{0.67 Ca^{2/3}}{\delta_0/D} - 3.35 Ca^{2/3}. \tag{12}$$

Fig. 17 Dimensionless liquid film thickness (δ_0/D) against dimensionless viscous boundary layer thickness $(\nu L/U)^{1/2}/D$.
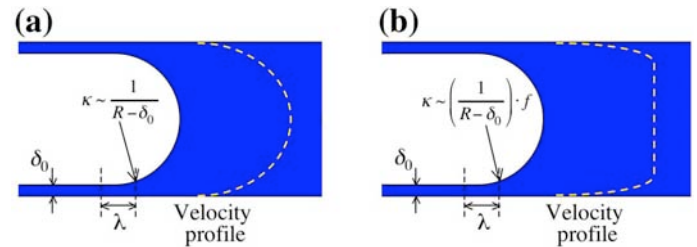

Fig. 18 Schematic diagram of velocity profiles: (a) steady condition - zero acceleration (b) acceleration condition.

In order to express the bubble acceleration effect, Bond number based on the bubble acceleration is introduced. The bubble acceleration is simply expressed with the assumption of uniform acceleration as follows:

$$Bo = \frac{\rho a D^2}{\sigma}, \quad (13)$$

$$a = \frac{U^2}{2L}. \quad (14)$$

Figure 19 shows the relationship between R.H.S. of Eq. (12) and the Bond number. Only the experimental data that deviate from the zero acceleration case are used. All the data are well correlated with a single line,

$$f = 0.692 Bo^{0.414}. \quad (15)$$

Substituting Eq. (15) in Eq. (11), a correlation for the liquid film thickness under bubble acceleration can be obtained as follows:

$$\frac{\delta_0}{D} = \frac{0.968 Ca^{2/3} Bo^{-0.414}}{1 + 4.838 Ca^{2/3} Bo^{-0.414}}. \quad (16)$$

Figures 20 and 21 show the comparison between the experimental data and the prediction of Eq. (16). As shown in Fig. 21, the present correlation can predict the liquid film thickness within the range of ±10 % accuracy.

4. CONCLUSIONS

Liquid film thickness in micro tube under wall superheat and bubble acceleration was investigated. It is observed that if the wall superheat becomes larger than 5°C, liquid film thickness becomes smaller than the adiabatic prediction due to the decrease of viscosity near the wall. It is confirmed that the empirical correlation proposed in the previous study [1] is still applicable for the case of the high wall superheat if the wall temperature is used for the viscosity. When the bubble is accelerated, viscous boundary layer strongly affects the liquid film thickness. If the viscous boundary layer is thick, liquid film thickness can be determined by the steady state prediction, Eq. (4). However, if the viscous boundary layer is thin, liquid film thickness is restricted by the viscous boundary layer. Experimental correlation for the liquid film thickness under bubble acceleration is proposed in terms of capillary number and Bond number. The present correlation can predict the liquid film thickness within the range of ±10 % accuracy. In order to develop precise flow boiling models in a micro tube, it is necessary to consider the effect of the wall superheat as well as the bubble acceleration effect on the liquid film thickness.
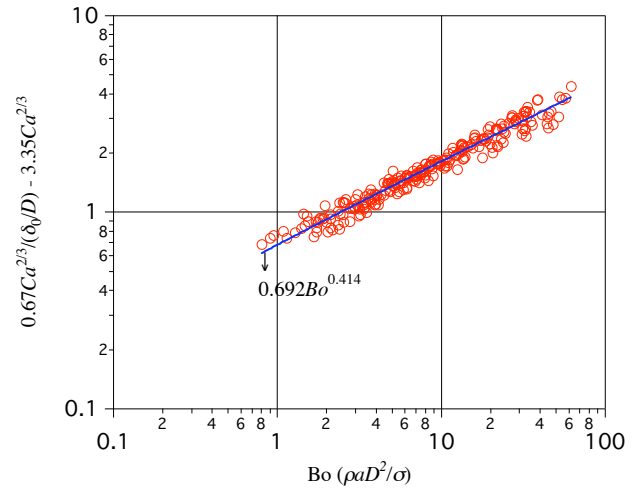
Fig. 19 R.H.S. of Eq. (12) against Bond number ($\rho a D^2/\sigma$).
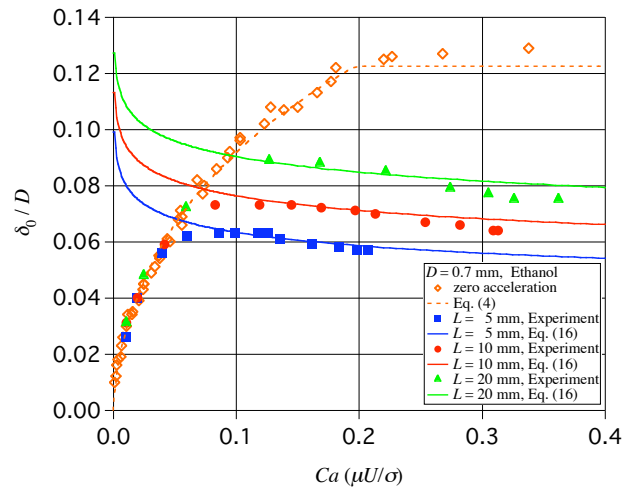

Fig. 20 Predicted liquid film thickness (δ_0/D) against capillary number ($Ca = \mu U/\sigma$) using ethanol, $D = 0.7$ mm.
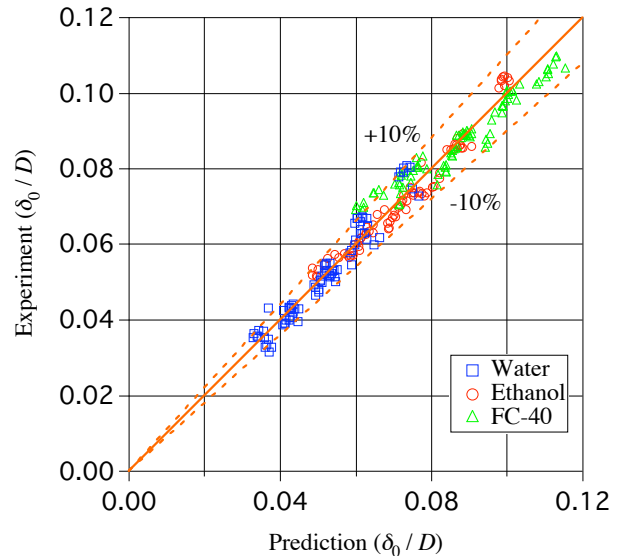

Fig. 21 Comparison between prediction and experimental results.

REFERENCES

[1] Han, Y. B. and Shikazono N., 2009, "Measurement of the liquid film thickness in micro tube slug flow," accepted to Int. J. Heat Fluid Flow.

[2] Kenning, D. B. R., Wen, D. S., Das, K. S. and Wilson, S. K., 2006, "Confined growth of a vapour bubble in a capillary tube at initially uniform superheat: Experiments and modeling," Int. J. Heat Mass Transfer, **49**, pp. 4653-4671.

[3] Thome, J. R., Dupont, V. and Jacobi, A. M., 2004, "Heat transfer model for evaporation in micro channels. Part I: presentation of the model," Int. J. Heat Mass Transfer, **47**, pp. 3375-3385.

[4] Taylor, G. I., 1961, "Deposition of a viscous fluid on the wall of a tube," J. Fluid Mech., **10**, pp. 161-165.

[5] Bretherton, F. P., 1961, "The motion of long bubbles in tubes," J. Fluid Mech., **10**, pp. 166-188.

[6] Moriyama, K. and Inoue, A., 1996, "Thickness of the liquid film formed by a growing bubble in a narrow gap between two horizontal plates," Trans. of the ASME, **118**, pp. 132-139.

[7] Heil, M., 2001, "Finite Reynolds number effects in the Bretherton problem," Phys. of Fluids, **13**, pp. 2517-2521.

[8] Aussillous, P. and Quere, D., 2000, "Quick deposition of a fluid on the wall of a tube," Phys. of Fluids, **12**, pp. 2367-2371.

[9] Kreutzer, M. T., Kapteijn, F., Moulijn, J. A., Kleijn, C. R. and Heiszwolf, J. J., 2005, "Inertial and interfacial effects on pressure drop of Taylor flow in capillaries," AIChE J., **51**, pp. 2428-2440.

[10] Utaka, Y., Okuda, S. and Tasaki, Y., 2007, "Structure of micro-layer and characteristics of boiling heat transfer in narrow gap mini-channel system," Trans. of the JSME, Series B, **73**, pp. 1929-1935.

[11] Hazuku, T., Fukamachi, N., Takamasa, T., Hibiki, T. and Ishii, M., 2005, "Measurement of liquid film in microchannels using a laser focus displacement meter," Experiments in Fluids, **38**, pp. 780-788.

[12] Takamasa, T. and Kobayashi, K., 2000, "Measuring interfacial waves on film flowing down tube inner wall using laser focus displacement meter," J. Multiphase Flow, **26**, PP. 1493-1507.